Cell Death & Differentiation (2018) 25:951–965
https://doi.org/10.1038/s41418-017-0031-1

Cell Death & Differentiation

ARTICLE

Necroptotic signaling is primed in *Mycobacterium tuberculosis*-infected macrophages, but its pathophysiological consequence in disease is restricted

Michael D. Stutz[1,2] · Samar Ojaimi[1,2] · Cody Allison[1,2] · Simon Preston[1,2] · Philip Arandjelovic[1,2] · Joanne M. Hildebrand[2,3] · Jarrod J. Sandow[2,4] · Andrew I. Webb[2,4] · John Silke[2,3] · Warren S. Alexander[2,5] · Marc Pellegrini[1,2]

Received: 24 May 2017 / Revised: 14 September 2017 / Accepted: 25 October 2017 / Published online: 11 December 2017
© The Author(s) 2018. This article is published with open access

Abstract

Mixed lineage kinase domain-like (MLKL)-dependent necroptosis is thought to be implicated in the death of mycobacteria-infected macrophages, reportedly allowing escape and dissemination of the microorganism. Given the consequent interest in developing inhibitors of necroptosis to treat *Mycobacterium tuberculosis* (Mtb) infection, we used human pharmacologic and murine genetic models to definitively establish the pathophysiological role of necroptosis in Mtb infection. We observed that Mtb infection of macrophages remodeled the intracellular signaling landscape by upregulating MLKL, TNFR1, and ZBP1, whilst downregulating cIAP1, thereby establishing a strong pro-necroptotic milieu. However, blocking necroptosis either by deleting *Mlkl* or inhibiting RIPK1 had no effect on the survival of infected human or murine macrophages. Consistent with this, MLKL-deficiency or treatment of humanized mice with the RIPK1 inhibitor Nec-1s did not impact on disease outcomes *in vivo*, with mice displaying lung histopathology and bacterial burdens indistinguishable from controls. Therefore, although the necroptotic pathway is primed by Mtb infection, macrophage necroptosis is ultimately restricted to mitigate disease pathogenesis. We identified cFLIP upregulation that may promote caspase 8-mediated degradation of CYLD, and other necrosome components, as a possible mechanism abrogating Mtb's capacity to coopt necroptotic signaling. Variability in the capacity of these mechanisms to interfere with necroptosis may influence disease severity and could explain the heterogeneity of Mtb infection and disease.

Introduction

Mycobacterium tuberculosis (Mtb) subverts numerous macrophage cellular pathways in order to exploit the cell as a replicative niche [1]. The manipulation of host programmed cell death pathways by Mtb, and the consequence of this on the outcome of the infection, remains highly controversial. Several studies, predominantly using immortalized murine macrophages, reported that apoptosis was induced exclusively by virulent Mtb strains [2–5]. A zebrafish study of *Mycobacterium marinum* infection supported this, and suggested that the subsequent phagocytosis of apoptotic cells expanded the pool of infected cells [6]. However, other observations contradict this, with virulent Mtb inducing less apoptosis than avirulent strains, in experiments using principally immortalized and primary human cells [7–12]. These discrepancies most likely reflect experimental variability between studies, particularly in terms of the species of origin and mortality of cells and their

Edited by T. Mak

Electronic supplementary material The online version of this article (https://doi.org/10.1038/s41418-017-0031-1) contains supplementary material, which is available to authorized users.

✉ Marc Pellegrini
pellegrini@wehi.edu.au

1 Division of Infection and Immunity, The Walter and Eliza Hall Institute of Medical Research, Parkville, VIC 3052, Australia

2 Department of Medical Biology, The University of Melbourne, Parkville, VIC 3010, Australia

3 Division of Cell Signalling and Cell Death, The Walter and Eliza Hall Institute of Medical Research, Parkville, VIC 3052, Australia

4 Division of Systems Biology and Personalised Medicine, The Walter and Eliza Hall Institute of Medical Research, Parkville, VIC 3052, Australia

5 Division of Cancer and Haematology, The Walter and Eliza Hall Institute of Medical Research, Parkville, VIC 3052, Australia

ability to retain particular molecular pathways in culture, as well as differences in bacterial strains and experimental endpoints. Nonetheless, the identification of virulence genes in Mtb that abrogate apoptotic signaling supports the prevailing opinion that apoptosis of infected macrophages is protective for the host and is thus inhibited by virulent Mtb [13–18]. Some groups additionally reported that macrophages underwent a lytic death at late stages of infection or at high multiplicity of infection (MOI) [19, 20]. Consistent with this, a study of *M. marinum* infection of zebrafish reported that macrophages infected with these mycobacteria are stimulated by host TNF to die by a programmed form of lytic cell death termed necroptosis [21]. Recently, it was reported that siRNA silencing of mixed lineage kinase domain-like (MLKL), the essential mediator of necroptosis [22, 23], rescues much of the death of Mtb-infected macrophages *in vitro*, although it was not definitive whether the death that occurred in MLKL-sufficient cells was indeed necroptosis [24]. It has been proposed that lytic death benefits mycobacteria by enabling escape into the growth-permissive extracellular microenvironment [25]. Collectively, these studies established the current view that Mtb initially inhibits macrophage apoptosis to allow replication, while at later stages induces a lytic death such as necroptosis to escape the host cell and disseminate. The reported pathophysiological function of necroptosis in *M. marinum* infection of zebrafish has been a major contributor in shaping this current dogma in the Mtb field. This is despite the fact that the observations have not been confirmed in a mammalian *in vivo* model of Mtb infection, and it is thus unclear whether they translate to Mtb.

Death via necroptosis can be induced by ligation of TNF receptor 1 (TNFR1) by TNF, which is abundant during Mtb infection [26, 27]. Receptor interacting protein kinase 1 (RIPK1) normally promotes cell survival downstream of TNFR1 ligation by engaging the NF-κB pathway. This depends upon its ubiquitination by the cellular inhibitor of apoptosis (cIAP) proteins. The absence of optimal RIPK1 ubiquitination (for example, due to the loss of cIAPs) allows RIPK1 to associate with caspase 8, resulting in apoptosis. However, when caspase 8 is absent or inhibited, RIPK1 and RIPK3 can interact and autophosphorylate. Phosphorylated RIPK3 can then bind and phosphorylate MLKL, which oligomerizes and translocates to the cell membrane to execute necroptotic death [28–32]. Additionally, RIPK3 can be activated to induce necroptosis by the cytoplasmic DNA sensor Z-DNA binding protein 1 (ZBP1; also known as DAI or DLM1) [33] and downstream of Toll-like receptors by TIR domain-containing adapter-inducing interferon-β (TRIF) [34]. A function of necroptosis in microbial infections is supported by several reports describing pathogen-derived molecules that modulate necroptotic signaling and either induce or inhibit host cell necroptosis [33, 35–38]. One report suggests that Mtb actively suppresses/constrains caspase 8 activity [39], and this would support the notion that Mtb preferentially promotes necroptosis and down-regulates apoptosis during disease pathogenesis.

Several groups are pursuing the development of therapeutics targeting necroptosis, and particularly MLKL, for infectious and non-infectious diseases in which necroptosis has been implicated. The recent report describing a pathological function of necroptosis in *M. marinum* infection has spurred tremendous interest in the development and application of such inhibitors clinically for the treatment of tuberculosis [21, 25]. It is therefore critically important to establish the precise role of MLKL specifically in Mtb infection. Our study addresses this substantial gap in our understanding of the pathophysiology of Mtb infection by using genetic tools and *in vivo* aerosolized infection of both conventional and humanized mice.

Results

Mtb-infected macrophages are primed for necroptosis

We examined whether the essential components of the necroptotic pathway were present and/or differentially regulated in macrophages upon Mtb infection *in vitro*. A consistent, sustained upregulation of MLKL protein was observed as early as 24 h post-infection, at both low and high MOI (Fig. 1a). We also observed a striking reduction in cIAP1 and cylindromatosis (CYLD) levels, particularly at high MOI, together with an increase in TNFR1, cellular FLICE-inhibitory protein (cFLIP) and ZBP1, while the expression of caspase 8, RIPK1, and RIPK3 were not consistently altered by Mtb infection (Fig. 1a).

To determine whether these changes in protein expression occurred *in vivo*, we isolated alveolar macrophages from bronchoalveolar lavage of both uninfected and Mtb-infected mice. Macrophages from infected mice showed approximately 7-fold upregulation of MLKL (Fig. 1b). Similarly, TNFR1, cFLIP, and ZBP1 expression was strongly increased, while CYLD was reduced and caspase 8, RIPK1 and RIPK3 were unaltered. Although we did not observe any differences in cIAP1 level between uninfected and infected macrophages *in vivo*, the data overwhelmingly supported the *in vitro* results.

MLKL upregulation in Mtb infection is induced by IFNs

Previous work suggested that cytokines upregulate protein levels of necroptotic signaling molecules [40]. We therefore hypothesized that the upregulation of MLKL in Mtb-infected BMDMs was mediated by cytokine signaling. To test this, we

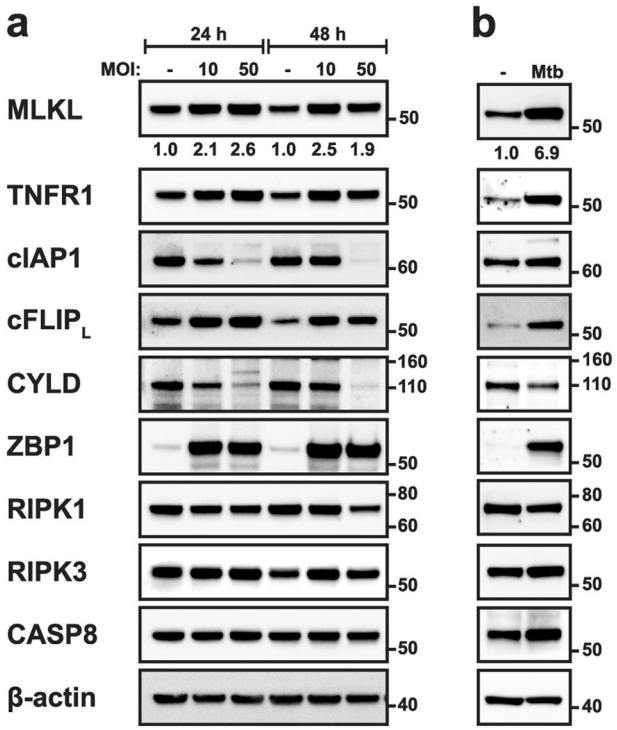

Fig. 1 Macrophages infected with Mtb are primed for necroptosis. a Western blot analysis of necroptosis-associated proteins in wild-type BMDMs infected with Mtb for 24 h or 48 h. Representative of four independent experiments. **b** Western blot analysis of MLKL levels in alveolar macrophages isolated from the BAL of both uninfected and Mtb-infected wild-type mice (three–four weeks post-infection). Lysates from three uninfected and three infected mice were pooled. Representative of two experiments. Protein levels relative to uninfected samples at each time point (and adjusted for actin loading) were quantitated by densitometry for certain panels, and appear below the panel to which they relate. Numbers to the right of the panels represent the positions of protein size markers (in kDa)

treated naïve BMDMs with TNF or type I IFN (IFNβ), which are produced by macrophages during Mtb infection. We also treated cells with type II IFN (IFNγ), given that this (primarily) $CD4^+$ T cell-derived cytokine is critical in the immune response to Mtb infection. Both IFNβ and IFNγ induced a similar degree of MLKL upregulation as Mtb infection (Supplementary Fig. 1a). BMDMs from *Ifnar1*$^{-/-}$ mice, which lack the type I IFN receptor, failed to upregulate MLKL upon infection (Supplementary Fig. 1b), demonstrating that macrophages were capable of upregulating MLKL through autocrine/paracrine type I IFN signaling, independent of lymphocyte-derived IFNγ, despite both being capable of mediating this.

Necroptosis is induced experimentally by stimulating TNFR1 in the presence of SMAC mimetics (to deplete cIAPs) as well as caspase inhibitors (to prevent apoptosis), and requires MLKL [41]. The deubiquitinase CYLD has been claimed to be required for necroptosis [40, 42]. Therefore, our data provides qualified support for the notion that Mtb-infected macrophages, *in vitro* and *in vivo*, may be primed to undergo necroptotic death, with the exception of our finding that CYLD protein levels were strongly suppressed which, according to recent reports, impedes the induction of necroptosis. The obvious and critical question is, does necroptosis prevail in Mtb infection as the literature would suggest?

Necroptosis of Mtb-infected macrophages is restricted

To explore whether Mtb infection did in fact induce macrophage necroptosis, we examined RIPK3-mediated phosphorylation of MLKL—a key event in the activation of necroptosis [32]. However, we were unable to detect phosphorylated (p) MLKL in either infected BMDMs (Fig. 2a) or alveolar macrophages from Mtb-infected mice (Fig. 2b). Processing of the apoptotic caspases 3 and 8, indicating their activation, was also undetectable (Fig. 2a). Thus, we were unable to detect markers of either necroptosis or apoptosis, despite observing cell death in an MOI-dependent manner (Fig. 2c). We postulated that the inability to detect pMLKL may have reflected the potentially transient nature of MLKL phosphorylation, as well as the probable temporal variability in the death of individual cells. We therefore infected BMDMs from both wild-type and MLKL-deficient (*Mlkl*$^{-/-}$) mice and quantitated the amount of death. Surprisingly, we observed no difference in the proportion of *Mlkl*$^{-/-}$ BMDMs dying following Mtb infection compared to wild-type cells, suggesting that death was occurring in an MLKL-independent, non-necroptotic manner (Fig. 2c). To address the possibility that there were insufficient death ligands secreted by BMDMs to induce necroptosis, we added TNF 24 h post-infection. However, even with this treatment there were no substantial differences in the proportion of dead wild-type and *Mlkl*$^{-/-}$ BMDMs (Fig. 2d). It remained possible that infected macrophages were in fact undergoing necroptosis but, in the absence of MLKL, switched to apoptosis, leading to a similar amount of total cell death. However, treatment of wild-type or *Mlkl*$^{-/-}$ BMDMs with caspase inhibitor (Q-VD-OPh), to prevent either apoptosis or both apoptosis and necroptosis, respectively, did not substantially alter the proportion of cells dying from Mtb infection (Supplementary Fig. 2a), suggesting that substitution of cell death programs was not occurring.

We extended these findings to primary human monocytes which, similar to BMDMs, are sensitive to both apoptotic and necroptotic stimuli (Supplementary Fig. 3a and 3b). Viability decreased in an MOI-dependent manner similar to BMDMs (Fig. 2e). However, the extent of cell death was not significantly altered by treatment with the RIPK1 kinase inhibitor necrostatin-1 stable (Nec-1s) [43, 44] (Fig. 2e). Treatment of cells with TNF after infection also did not cause any difference in viability between vehicle and Nec-1s treated cells (Fig. 2f).

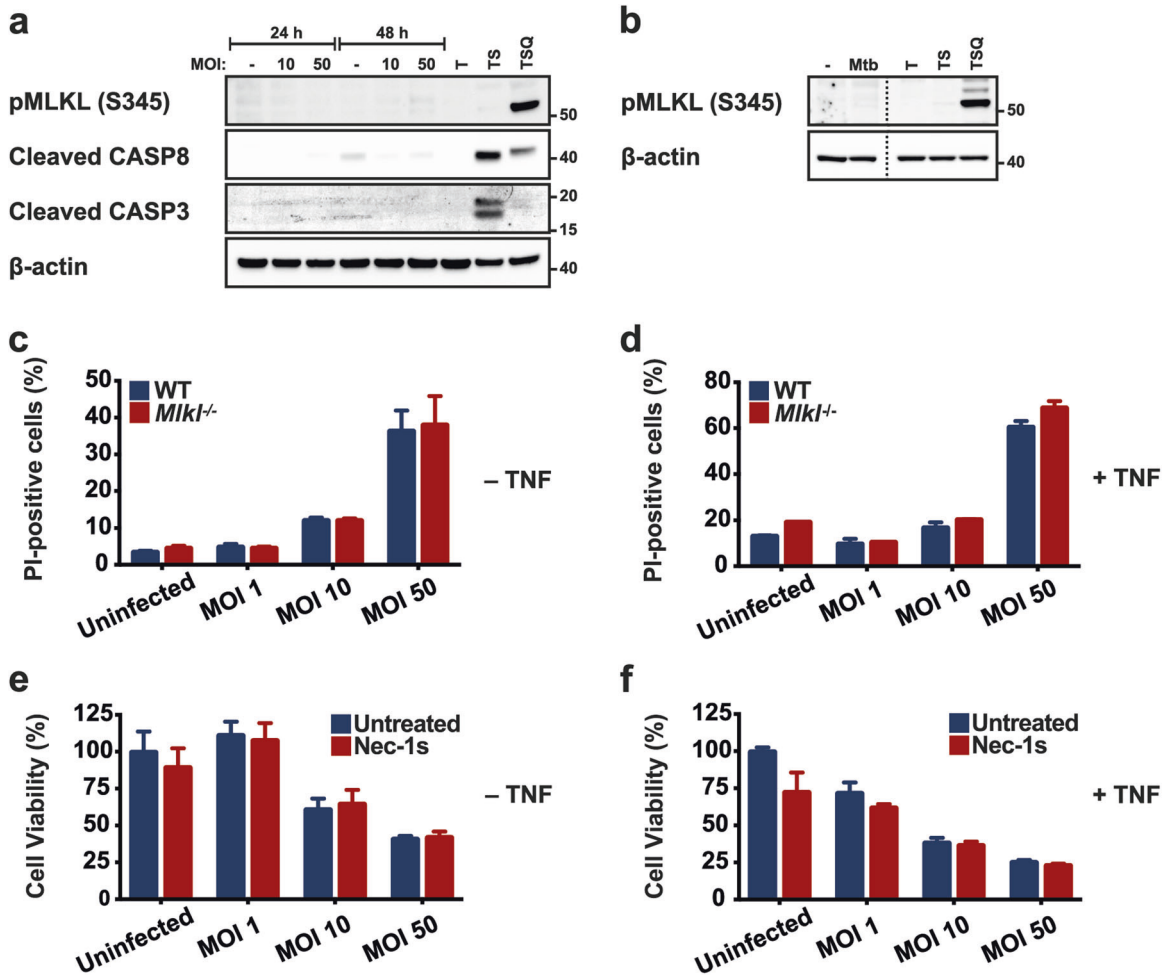

Fig. 2 Necroptotic death of Mtb-infected macrophages is restricted. a Western blot analysis of markers of programmed cell death in wild-type BMDMs infected with Mtb for 24 h or 48 h. Controls were prepared by treating uninfected BMDMs with either TNF (100 ng/ml), TNF and birinapant (10 μM), or TNF, birinapant and Q-VD-OPh (40 μM) for 24 h. Numbers to the right of the panels represent the positions of protein size markers (in kDa). Representative of three independent experiments. Abbreviations are as follows: T, TNF; S, SMAC mimetic (birinapant); Q, Q-VD-OPh. **b** Western blot analysis of phosphorylated MLKL in alveolar macrophages isolated from the BAL of uninfected and Mtb-infected wild-type mice. Controls were prepared as in (**a**). Lysates from three uninfected and three infected mice were pooled, and data are representative of two experiments. Vertical dashed lines indicate the positions where lanes that were not contiguous on the blot were juxtaposed to remove unused lanes. **c**, **d** Death of wild-type and *Mlkl*$^{-/-}$ BMDMs infected with Mtb for 48 h. BMDMs were either (**c**) untreated or (**d**) treated with 50 ng/ml TNF at 24 h post-infection. The amount of cell death was determined by PI staining and flow cytometry. Graphs show mean and SEM, and data were pooled from three biologically independent experiments. There were no statistically significant differences between genotypes in infected groups ($p > 0.05$; *t* test). **e**, **f** Death of primary human monocytes treated with either vehicle (DMSO) or Nec-1s (70 μM) and infected with Mtb for 24 h. Additionally, cells were either (**e**) untreated or (**f**) treated with 50 ng/ml TNF at 6 h post-infection. The amount of cell death was determined by MTS assay. Graphs show mean and SEM of triplicate wells. Representative of three biologically independent experiments. There were no statistically significant differences between vehicle and Nec-1s-treated cells ($p > 0.05$; *t* test)

Our data indicated that although Mtb infection primes certain components of the necroptotic pathway, this form of programmed cell death does not contribute to the attrition of Mtb-infected macrophages *in vitro*. It thus remained unclear which point in the necroptotic pathway was blocked to prevent necroptosis. Previous reports suggested that Mtb inhibits caspase 8 function [39]. Engagement of the apoptotic pathway by a Death Ligand such as TNF, while caspase 8 is inhibited, can lead to the activation of the necroptotic pathway. When Mtb-infected BMDMs were treated with TNF, we did not observe the same extent of RIPK1 phosphorylation (Supplementary Fig. 4a) or post-translational modification of RIPK3 (Supplementary Fig. 4b) as the positive control for necroptosis. This suggested that necroptosis was being restricted either at, or upstream of, necrosome assembly. It is therefore possible that either the necroptosis-

inhibitory function of caspase 8 remains active, or Mtb infection prevents engagement of the apoptotic pathway and therefore acts upstream of caspase 8 activation.

The loss of necroptotic signaling and its impact on Mtb disease pathogenesis in vivo

We hypothesized that the lack of necroptosis in Mtb-infected macrophages *in vitro*, despite priming for this form of death, may be attributable to the absence of the required ligands *in vitro*. We therefore examined the role of necroptosis *in vivo* using *Mlkl*$^{-/-}$ mice. The bacterial burden in the lungs and spleens of *Mlkl*$^{-/-}$ mice was indistinguishable from that of wild-type mice at all time points (Fig. 3a and b). The similarity in bacterial burden was consistent with the gross lung histopathology (Fig. 3c and Supplementary Fig. 5), which revealed a comparable number and size of inflammatory lesions (Fig. 3d) comprising dense aggregates of infiltrating immune cells.

MLKL does not contribute to the immunological response to Mtb infection

We considered the possibility that MLKL deficiency may affect macrophage function and/or other facets of immunity, thereby offsetting any potential benefits, as the literature would suggest, of interrupting necroptosis signaling during Mtb infection. An important mechanism that macrophages use to kill intracellular Mtb is the induction of iNOS [45]. However, the expression of iNOS following infection was comparable between wild-type and *Mlkl*$^{-/-}$ BMDMs (Supplementary Fig. 2b). Furthermore, there were no differences in the number of macrophages, granulocytes, dendritic cells, B cells or CD4^{+} and CD8^{+} T cells in either the lungs or spleen between infected wild-type and *Mlkl*$^{-/-}$ mice (Figs. 4a and 5a, Supplementary Fig. 6a), or in the organization of macrophages and T cells within pulmonary lesions (Figs. 4b, c and 5a, Supplementary Fig. 7). Consistent with this, there were no differences in either the concentration of TNF and IL-1β in lung homogenates (Fig. 4d), or in the number or percentage of Mtb early secreted antigenic target (ESAT)-6-specific, IFNγ/TNF-producing CD4^{+} T cells in either the lungs or spleens (Fig. 5c and Supplementary Fig. 6b). Collectively, these data indicated that MLKL deficiency did not alter the inflammatory and immune responses associated with Mtb infection.

Inhibition of necroptosis in humanized mice does not affect Mtb disease progression

We sought to confirm the human translatability of our *in vivo* data by using a robust humanized mouse model of Mtb infection. NOD scid gamma (NSG) mice reconstituted with human cord blood stem cells (humanized mice) recapitulate characteristics of human immunity, including innate and adaptive cells. We used Nec-1s to block necroptosis *in vivo*. Nec-1s shows enhanced metabolic stability and excellent selectivity toward RIPK1 inhibition [43, 44], and has been used *in vivo* in several recent publications [46–49]. Nonetheless, we firstly confirmed that the dose of Nec-1s we used efficiently inhibited necroptosis of human cells *in vivo* by infecting humanized mice with lymphocytic choriomeningitis virus (LCMV). This results in a TNF-mediated immune response which is maximal around seven days post-infection. At that time, we treated mice with caspase inhibitors (emricasan), either alone or in combination with Nec-1s, followed by the IAP antagonist birinapant. Mice receiving emricasan without Nec-1s developed acute illness 3 h after birinapant treatment, characterized by ruffled fur, diarrhea and non-responsiveness. We noted a clear and substantial reduction in the amount of positive staining for human pMLKL [32] in spleens from mice receiving both emricasan and Nec-1s compared with those receiving only emricasan (Supplementary Fig. 8), indicating efficient inhibition of necroptosis of human cells with Nec-1s *in vivo*.

We pre-treated humanized mice with Nec-1s 18 h and 1 h prior to Mtb infection, and then administered daily doses until mice were sacrificed at day 10 post-infection. We found similar bacterial burdens in the lungs and spleens of vehicle and Nec-1s treated mice (Fig. 6), demonstrating that the inhibition of necroptosis in humanized mice did not impair the control or dissemination of Mtb.

Discussion

Recent work suggested the induction of macrophage necroptosis as a strategic maneuver by Mtb to facilitate host cell escape and dissemination. Our data challenges this view, and shows convincingly that necroptotic signaling is restricted and does not contribute to Mtb infection-associated host cell death over and above other forms of cell death *in vitro* and *in vivo*.

It was somewhat surprising to find that Mtb infection of macrophages *in vitro* appeared to skew the intracellular signaling milieu so as to poise the cell for necroptosis. The increase in TNFR1 expression may sensitize infected cells to TNF-mediated death. We previously reported a similar upregulation in hepatitis B virus-infected hepatocytes *in vivo* [50]. We also noted a substantial increase in ZBP1 expression, which may sensitize cells to necroptosis following detection of cytoplasmic Mtb DNA. Furthermore, cIAP1 levels were drastically reduced in Mtb-infected BMDMs, particularly at high MOI. The cIAP molecules are usually antagonized genetically or with SMAC mimetics to experimentally induce

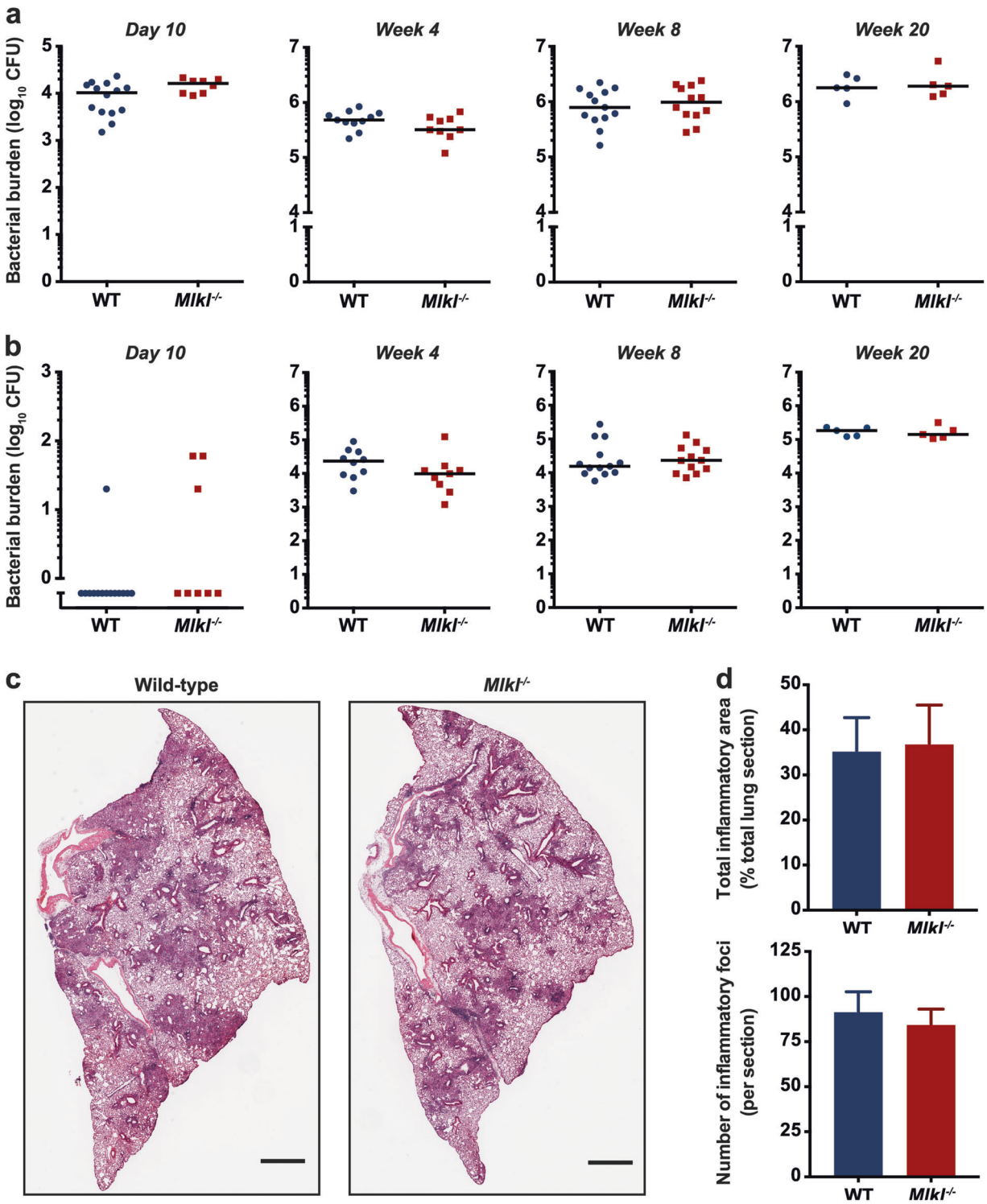

Fig. 3 Loss of MLKL does not affect the control and progression of Mtb infection *in vivo*. a–d Wild-type and *Mlkl*$^{-/-}$ mice were infected with Mtb by aerosol, and sacrificed at the indicated times post-infection. **a** Lungs and **b** spleens were homogenized and plated on 7H11 agar plates to enumerate CFU per organ. Horizontal bars indicate the median and each point represents one mouse. Data were pooled from two (week four and eight) or three (day 10) independent experiments ($n = 8$–14 per group). There were no statistically significant differences between genotypes ($p > 0.05$; t test). **c** Lung histology of mice four weeks post-infection. Sections of the left lobe were stained with H&E. Representative of 12 mice of each genotype. Scale bar represents 1 mm. **d** Quantitation of H&E-stained lung sections in terms of both the percentage of the total section surface area comprising inflammatory areas (upper), as well as the number of inflammatory areas per section (lower). Graphs show mean and SEM of pooled data from two independent experiments ($n = 10$ per group). There were no statistically significant differences between genotypes ($p > 0.05$; Mann–Whitney test)

necroptosis. The physiological conditions that elicit necroptosis during certain infections are not well characterized. To our knowledge, inhibition of cIAPs following infection has not previously been demonstrated, and may represent a novel mechanism by which Mtb primes necroptosis. Finally, we found an increase in MLKL expression, which was also reported recently [24]. We extended this finding by showing that the increase in MLKL levels could be stimulated by type I and type II IFN signaling. This is consistent with the reported role of type I IFNs in priming cells for necroptosis, at least partly by stimulating the expression of necroptosis signaling molecules including MLKL [40]. With the exception of cIAP1, the changes in protein expression in infected BMDMs were similar, and sometimes more striking, in alveolar macrophages from infected mice, demonstrating the relevance of these changes during physiological infection *in vivo*. The lack of a reduction in cIAP1 level *in vivo* was likely due to a much smaller proportion of macrophages becoming infected in the lung compared with *in vitro* conditions, such that any differences in infected cells could therefore not be resolved from a pool of predominantly uninfected cells. The downregulation in cIAP1 level may be dependent upon actual infection of cells with Mtb, while the other proteins we examined may be regulated by cytokine signaling, as we showed for MLKL.

Given this data, we expected Mtb-infected macrophages to die by necroptosis. However, the absence of detectable pMLKL, and the fact that genetic deletion of *Mlkl* did not rescue cells from death, suggested that MLKL-dependent necroptosis did not contribute to the death of Mtb-infected cells. Additionally, we did not detect any cleaved caspases, indicating that apoptosis was likely not a major contributor. We confirmed these results with primary human monocytes, in which blockage of necroptosis did not reduce the death of Mtb-infected cells. We corroborated this *in vivo* using MLKL-deficient mice, which had a similar degree of macrophage infiltration into the lungs during infection compared to wild-type mice. One could argue that the continual recruitment of new macrophages to the lung in wild-type mice masked the loss of these cells by necroptosis. However, the current literature suggests that this would manifest in more extensive pulmonary inflammation compared to *Mlkl*$^{-/-}$ mice, which we did not observe. Additionally, the histopathology and bacterial burdens in the lungs and spleens were indistinguishable between the strains of mice, arguing against the reported role for necroptosis in disseminating mycobacteria. We extended our studies to humanized mice, which is important given the potential species differences in the activity and regulation of cellular pathways. Humanized mice recapitulate many aspects of human TB disease [51]. We showed that the pharmacologic inhibition of necroptosis did not affect disease outcomes in humanized mice. While it remains possible that Nec-1s, through its targeting of RIPK1, may have inhibited other RIPK1-dependent forms of cell death, its ability to block MLKL-driven necroptosis was nevertheless not reflected in any phenotype *in vitro* or *in vivo*.

An intriguing aspect of our work is that Mtb primed, but ultimately failed to induce, macrophage necroptosis. This strongly suggested that necroptotic death was being restricted. Necroptosis requires that caspase 8 activity be constrained, but not abolished, since the autocleavage and homodimerization of caspase 8 following TNF ligation inactivates RIPK1 and RIPK3 and induces apoptosis. We found that caspase 8 levels were not reduced upon macrophage infection, but instead noted an increase in cFLIP, which normally heterodimerizes with uncleaved caspase 8. The best described function of these caspase 8/cFLIP heterodimers is to prevent the formation and activation of caspase 8 homodimers, and thereby inhibit apoptosis [52]. However, these heterodimers also retain sufficient catalytic function to cleave RIPK1, RIPK3, and CYLD and thereby also simultaneously inhibit activation of MLKL and the necroptotic pathway [53–56]. RIPK1 and RIPK3 levels appeared to be unaffected by Mtb infection, but we noted that CYLD was substantially reduced. CYLD functions primarily to remove certain ubiquitin chains from RIPK1 in the necrosome [42]. Since this deubiquitination has been reported to be necessary for RIPK1 and RIPK3 phosphorylation and function, the loss of CYLD protects cells from necroptosis [40, 42]. The ratio between cFLIP and caspase 8 is a critical determinant of cell fate [57]. Our data therefore supports the notion that the increased cFLIP expression during infection alters the stoichiometry of the caspase 8/cFLIP heterodimers to favor their proteolytic degradation of CYLD. This may be responsible for the failure of Mtb-infected macrophages to undergo necroptosis. However, loss of CYLD *in vivo* was shown to delay, but not prevent necroptosis during skin inflammation [58]. Furthermore, recent work showed that RIPK1 is not devoid of polyubiquitin chains once it has translocated to the necrosome [59]. Rather, it appears that a complex and poorly understood series of RIPK1 ubiquitination and deubiquitination events occur within the necrosome, and which are required for necrosome assembly and function. It is clear that additional molecules are at play, possibly novel phosphatases and E3 ligases, which have not been fully clarified. Nonetheless, we speculate that Mtb may have seconded necroptotic signaling for disease pathogenesis, but perhaps the host cell developed mechanisms to abrogate the activation of the necrosome and mitigate disease.

Regardless of the means by which necroptosis is restricted, our results contradict those of Roca and Ramakrishnan [21]. In their study, pharmacologic inhibitors of both MLKL and putative components of the necroptotic pathway were used to study necroptosis in *M. marinum*-infected zebrafish. It is noteworthy, however, that although

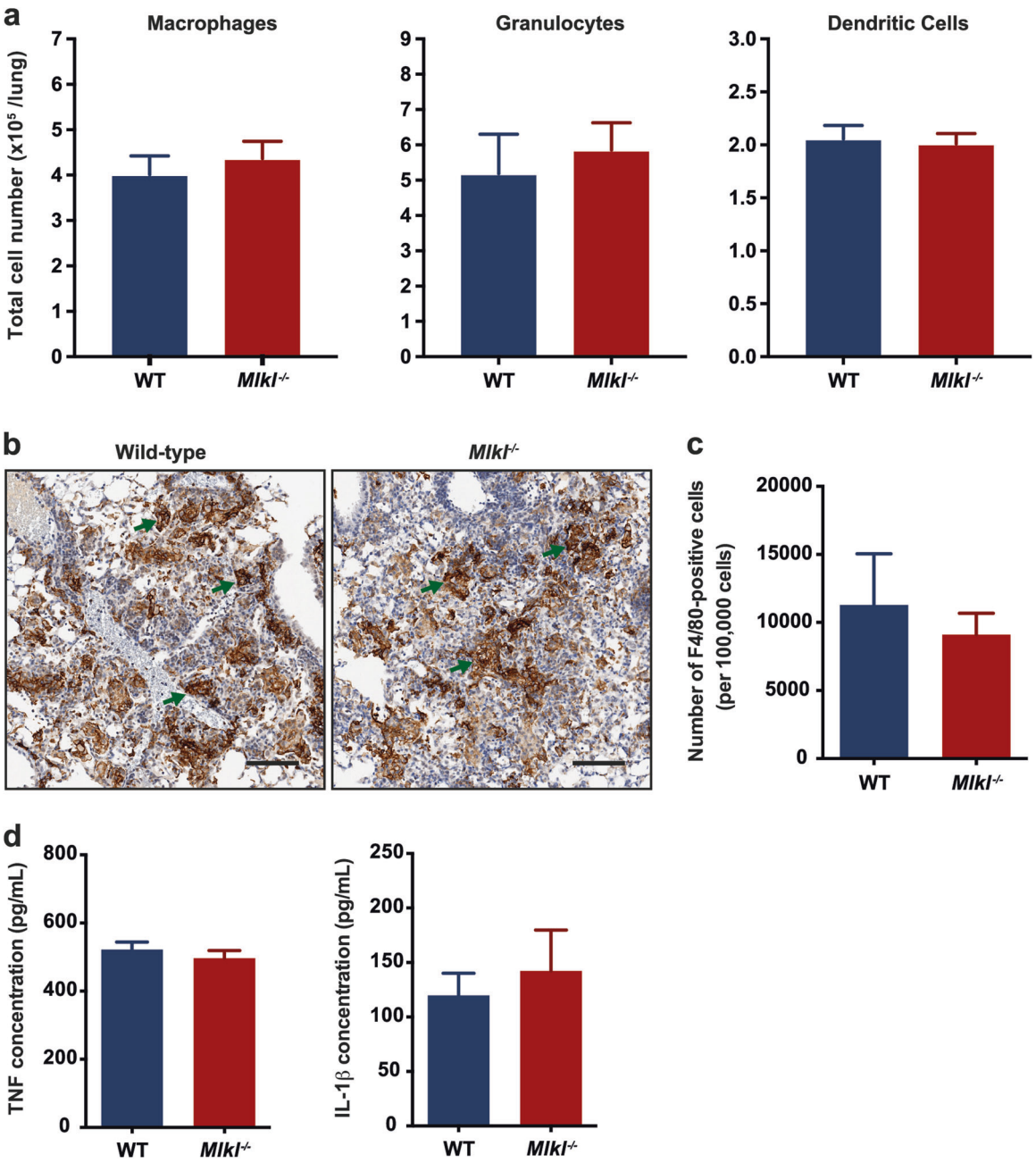

Fig. 4 Infiltration of innate immune cells into the lungs following Mtb infection is not affected by the loss of MLKL signaling. a Flow cytometric analysis of the total number of $CD11b^{+}Gr1^{lo}$ macrophages, $CD11b^{+}Gr1^{hi}$ granulocytes and $CD11c^{+}MHCII^{+}$ dendritic cells isolated from the lungs of mice four weeks after infection. **b** Immunohistochemical staining for F4/80 in lung sections from wild-type and $Mlkl^{-/-}$ mice sacrificed four weeks after infection, and **c** quantitation of the number of F4/80-positive cells per 100,000 cells. Arrows indicate examples of clusters of positive-stained cells. Representative of two independent experiments of $n = 3$–4 in each group. Scale bar represents 100 µm. **d** TNF and IL-1β levels quantitated by ELISA in the lung homogenates of mice four weeks after infection. Data were pooled from two independent experiments ($n = 9$–11 in each group). **a**, **b**, **d** Graphs show mean and SEM. There were no statistically significant differences between genotypes ($p > 0.05$; t test)

the authors were unable to identify a fish MLKL orthologue, they were able to inhibit cell death with an MLKL inhibitor that specifically inhibits human but not mouse MLKL [23]. Genetic targeting of *Mlkl*, the only essential downstream effector that has been conclusively identified, in species with a well-characterized necroptotic pathway, is undoubtedly the surer method to interrogate the role of necroptosis in Mtb infection. We believe that our gene-targeted approach using a physiologically relevant mammalian model of Mtb infection, in combination with our humanized mouse model, constitutes a more precise and thorough dissection of the role of necroptosis in this disease.

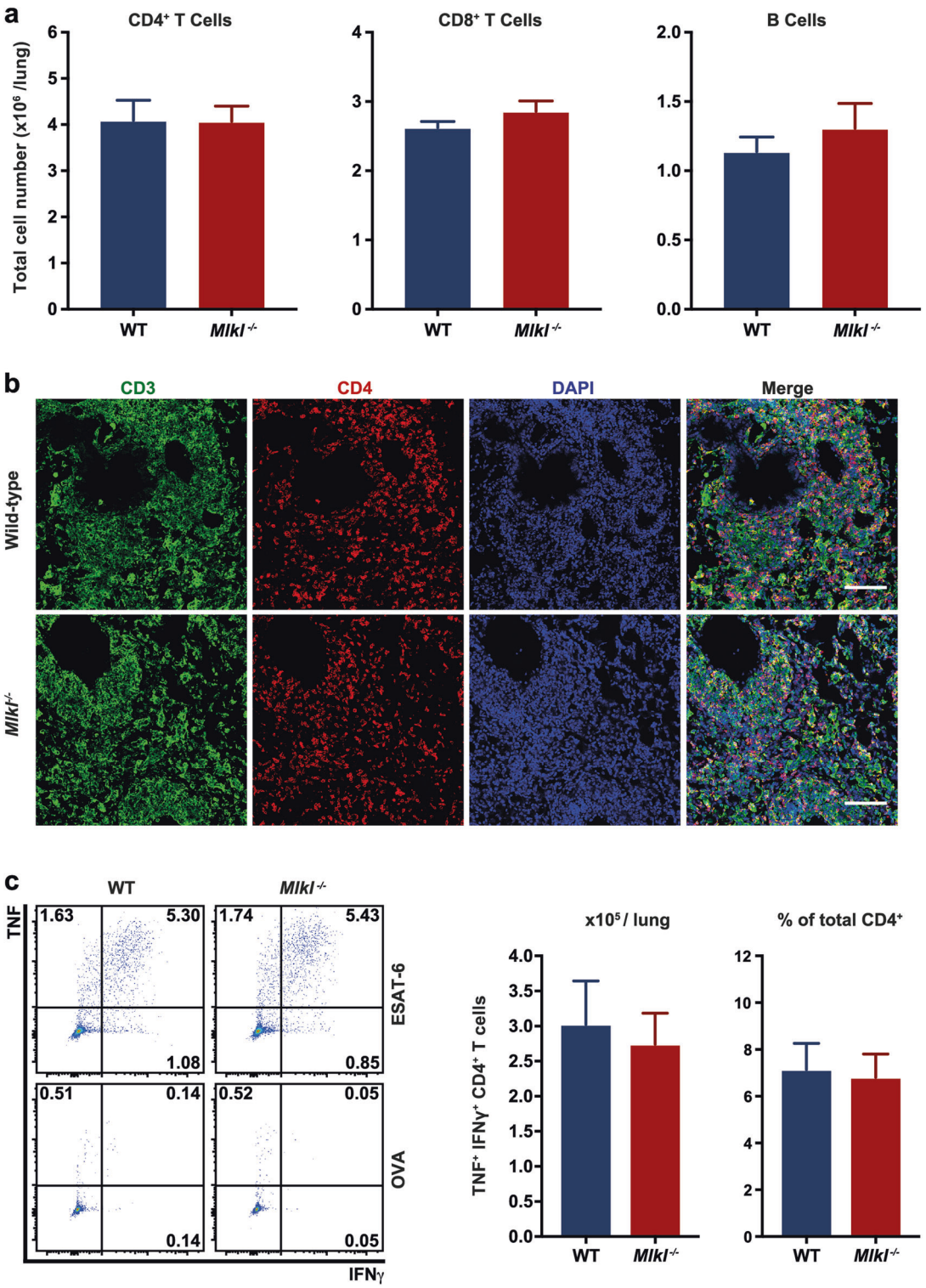

Fig. 5 The adaptive immunological response to Mtb infection *in vivo* is not perturbed by the loss of MLKL signaling. a Flow cytometric analysis of the total number of $CD4^+$ T cells, $CD8^+$ T cells and $CD19^+MHCII^+$ B cells isolated from the lungs of mice four weeks after infection. **b** Immunofluorescence staining (blue DAPI, green CD3 and red CD4) of lung sections from mice four weeks after infection. Representative of $n = 4$ in each group. Three inflammatory lesions were examined per mouse. Scale bar represents 100 µm. **c** Quantitation of the number of Mtb ESAT-6-specific $CD4^+$ T cells in the lungs of mice four weeks after infection. Cells were isolated from the lungs and restimulated *ex vivo* with either ESAT-6 or OVA peptide, and analyzed for TNF and IFNγ production by intracellular cytokine staining and flow cytometry. (left) Representative flow cytometry plots and (middle) quantitation of the total number of $TNF^+IFN\gamma^+CD4^+$ T cells and (right) their frequency expressed as a percentage of total $CD4^+$ T cells are shown. **a**, **c** Graphs show mean and SEM of pooled data from two independent experiments ($n = 6$ per group). There were no statistically significant differences between genotypes ($p > 0.05$; *t* test)

In summary, our data show that necroptosis is primed in Mtb-infected macrophages, but that necroptotic signaling is ultimately abrogated, thereby mitigating any pathophysiological role of necroptosis in tuberculosis. We speculate that differences in the ability to restrict necroptosis may contribute to the diversity of human host responses, disease severity, and clinical outcomes.

Materials and methods

Mice

The Walter and Eliza Hall Institute of Medical Research Animal Ethics Committee reviewed and approved all animal experiments. Six- to 10-week old C57BL/6, *Mlkl*$^{-/-}$ [28] and *Ifnar1*$^{-/-}$ [60] mice were used, and were age-matched and sex-matched in all experiments. Humanized mice were generated using NOD.Cg-*Prkdc*^{scid} *Il2rg*^{tm1Wjl}/SzJ (NSG) mice (originally from JAX), raised under specific pathogen-free conditions. One- to two-day old pups were irradiated (150 cGy) and injected with 5×10^4 CD34$^+$ cord blood stem cells (Stem Cell Technologies, Vancouver, Canada) via the facial vein. Mice were bled 16 weeks after transplantation and flow cytometry was used to determine the extent of reconstitution with human leukocytes. At least 50% of blood leukocytes were human CD45$^+$ in all mice used in experiments. Humanized mice were treated with 10 mg/kg necrostatin-1 stable (Nec-1s or 7-Cl-O-Nec-1; Merck, Billerica, MA, USA) by intraperitoneal (IP) injection 18 h and 1 h prior to infection, and then daily. Control mice were treated with vehicle (10% DMSO in PBS). Mice infected with Mtb were housed in individually-ventilated microisolator cages.

Bacterial strains and culture

M. tuberculosis strain H37Rv was obtained from Nicholas P West (University of Queensland, Australia). Mycobacteria were grown statically to late-log phase at 37 °C in Middlebook 7H9 medium (BD Biosciences, San Jose, CA, USA) supplemented with 0.5% (v/v) glycerol (Ajax Finechem, Taren Point, Australia), 0.02% (v/v) Tween-80 (Sigma-Aldrich, St. Louis, MO, USA) and 10% (v/v) ADC supplements (50 g/l bovine serum albumin [Bovogen Biologicals, East Keilor, Australia], 8.5 g/l NaCl, 20 g/l dextrose and 0.03 g/l catalase [all from Sigma-Aldrich]), and 1 ml aliquots were stored at −80 °C until use. Four to five days prior to infection, mycobacterial stocks were thawed, passed 10 times through a 27-gauge needle to disperse aggregated bacteria, and cultured as above. On the day of infection, mycobacterial cultures were pelleted by centrifugation and resuspended in PBS + 0.05% Tween-80.

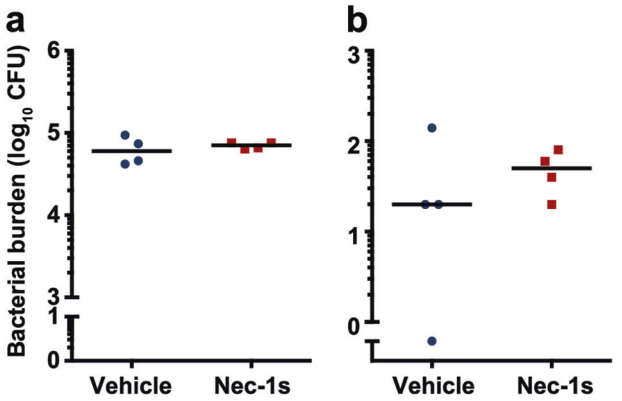

Fig. 6 Inhibition of necroptosis in humanized mice does not compromise control of bacterial growth or dissemination. a Nod scid gamma mice reconstituted with human cord blood stem cells (humanized mice) were treated with either vehicle or Nec-1s (10 mg/kg) both before and after infection with aerosolized Mtb (daily for an additional nine days post-infection) Lungs and **b** spleens were collected 10 days after infection, homogenized and plated on 7H11 agar plates to enumerate CFU per organ. Horizontal bars indicate the median and each point represents one mouse ($n = 4$ per group). There were no statistically significant differences between treatment groups ($p > 0.05$; *t* test)

To isolate single-celled Mtb, the suspension was then centrifuged at 130 *g* for 8 min to pellet aggregated mycobacteria. The supernatant (containing single-celled Mtb) was again pelleted and resuspended in either sterile water (for aerosolization) or PBS (for in vitro infections) to an optical density (590 nm) of 0.1–0.2. All procedures with viable Mtb were performed under biosafety level III conditions.

Cell culture, isolation, and stimulation

Bone marrow-derived macrophages (BMDMs) were prepared from WT, *Mlkl*$^{-/-}$ and *Ifnar1*$^{-/-}$ mice by flushing bone marrow from femurs and tibiae, and culturing cells in Dulbecco's modified Eagle's medium (DMEM) supplemented with 10% fetal bovine serum (FBS; Sigma-Aldrich), 15% L929-conditioned medium, 100 U/ml penicillin and 100 mg/ml streptomycin for six days in non-tissue culture treated dishes. Cells were then re-seeded into 10 cm dishes or 6-, 12- or 96-well plates at a density of 6.5×10^6, 1×10^6, 4×10^5 or 3.5×10^4 cells/well, respectively, in antibiotic-free medium and rested for 24 h before infection/treatment. In some experiments, BMDMs were treated with the indicated concentrations of recombinant mouse TNF (Biolegend, San Diego, CA, USA), IFNγ (Life Technologies, Carlsbad, CA, USA) or IFNβ. Apoptosis was induced with 50–100 ng/ml TNF and 10 μM of the bivalent SMAC mimetic birinapant (TetraLogic Pharmaceuticals). Necroptosis was induced by pre-treatment with either 40 μM Q-VD-OPh (Sigma-Aldrich) or 15 μM emricasan (also called

IDN-6556; MedKoo Biosciences, Chapel Hill, NC, USA) for 1 h before addition of TNF and birinapant, and inhibited by pre-treatment with 70 μM Nec-1s.

Primary human monocytes were isolated from the blood of healthy donors, which was obtained in the form of concentrated buffy packs (provided by the Australian Red Cross Blood Service, VIC, Australia). Peripheral blood mononuclear cells (PBMCs) were isolated by density gradient centrifugation using Ficoll-Paque (GE Healthcare, Piscataway, NJ, USA) and washed extensively with PBS. Serum was heat-inactivated at 60 °C for 30 min, centrifuged at 3270 *g* to pellet debris and filter sterilized (0.22 μm). Monocytes were separated by incubating PBMCs in 96-well plates for 90 min in Roswell Park Memorial Institute (RPMI) 1640 media with 7.5% autologous human serum (AHS) and penicillin/streptomycin. Non-adherent cells were removed and adherent monocytes washed thoroughly with PBS, before incubation in antibiotic-free macrophage-SFM media (Gibco, Mulgrave, Australia) containing 10% AHS. Cells were rested for 3 h before infection or treatment with the indicated stimuli. In some experiments, monocytes were pre-treated with 70 μM Nec-1s for 1 h prior to infection with Mtb. In all experiments, cells were incubated at 37 °C in a humidified incubator in the presence of 5% CO_2.

Macrophage infection

BMDMs and primary human monocytes were infected at various multiplicities of infection (MOIs) by adding single-cell Mtb suspension (prepared as described under 'Bacterial strains and culture') directly into the cell culture media. PBS was added to uninfected control cultures. After 3 h, the media were discarded, the cells washed with PBS to remove extracellular bacteria, and then cultured in fresh antibiotic-free media until harvest.

In vitro cell death determination

Viability of uninfected BMDMs and primary human monocytes following apoptotic and necroptotic stimuli was measured using the CellTiter-Glo Luminescent Cell Viability Assay (Promega, Madison, WI, USA), according to the manufacturer's instructions. To measure cell death of BMDMs infected with Mtb, both adherent and non-adherent cells were collected 48 h after infection. Cells were stained with 25 μg/ml propidium iodide (PI; Sigma-Aldrich) and analysed using a FACSAria Fusion flow cytometer (BD Biosciences). Death of primary human monocytes was determined 24 h after infection by MTS assay (CellTiter AQ_{ueous} One Solution Cell Proliferation Assay; Promega), according to the manufacturer's instructions.

Immunoprecipitation

BMDMs were cultured in 10 cm dishes and treated as indicated. Media was removed and plates washed with ice-cold PBS. Cells were lysed by scraping with cell lysis buffer containing 20 mM Tris-HCl, pH 7.5, 135 mM NaCl, 1.5 mM Mg_2Cl, 1 mM EGTA, 1% Triton X-100 (Sigma-Aldrich), 10% glycerol, EDTA-free protease inhibitor tablets (Roche, Basel, Switzerland), and phosphatase inhibitor tablets (Roche). Cell lysates were rotated at 4 °C for 20 min and then clarified at 4 °C at 14,000 rpm for 15 min. Protein G agarose beads (25 μl) were blocked for 1 h with 1% BSA in lysis buffer and then bound with 1.5 μg mouse anti-RIPK1 antibody (38/RIP; BD Biosciences). RIPK1 was immunoprecipitated with rotation at 4 °C for 4 h. Beads were washed four times with lysis buffer and eluted by heating to 95 °C in 50 μl of 2X NuPAGE LDS sample buffer (Life Technologies) containing 5% β-mercaptoethanol. Eluted proteins were subjected to Western blot analysis.

Western blots

Total cell protein was isolated from pelleted macrophages using cell lysis buffer. Absolute protein content of clarified lysates was determined by Bradford assay (Bio-Rad, Hercules, CA, USA), and equal quantities (20–50 μg) of total protein were separated under denaturing and reducing conditions (with 5% β-mercaptoethanol) using 4–12% SDS-PAGE gels (Life Technologies). Proteins were transferred onto nitrocellulose membranes, blocked with either 5% skim milk (Devondale, Brunswick, Australia) or 5% BSA (for phospho-proteins) in PBS with 0.05% Tween-20 (PBST) for 1 h, and detected using the following primary antibodies: rat anti-MLKL (3H1; available from Merck), rabbit anti-MLKL (phospho S345) (EPR9515[2]; Abcam, Cambridge, UK), rat anti-caspase 8 (3B10; WEHI), rabbit anti-cleaved caspase 8 (D5B2; Cell Signaling Technology), hamster anti-(mouse)TNFR1 (55R170; R&D Systems, Minneapolis, MN, USA), rat anti-cIAP1 (1E1-1-10; Enzo, Farmingdale, NY, USA), rat anti-cFLIP (Dave-2; AdipoGen, San Diego, CA, USA), rabbit anti-CYLD (D1A10; Cell Signaling Technology, Danvers, MA, USA), mouse anti-RIPK1 (38/RIP; BD Biosciences), rabbit anti-RIPK1 (phospho S166) (cat. #31122; Cell Signaling Technology), rabbit anti-RIPK3 (ProSci, Poway, CA, USA), mouse anti-ZBP1 (Zippy-1; AdipoGen), rabbit anti-cleaved caspase 3 (Asp175; Cell Signaling Technology), rabbit anti-iNOS (EPR16635; Abcam) and rabbit anti-β-actin (Cell Signaling Technology). HRP-conjugated goat secondary antibodies (Southern Biotech, Birmingham, AL, USA) were then applied to membranes, which were subsequently incubated with Amersham ECL Prime Western Blotting Detection

Reagent (GE Healthcare) and imaged using a ChemiDoc Touch Imaging System (Bio-Rad). Densitometry was performed using Image Lab v.5.2.1 software (Bio-Rad).

Aerosol infection

Mice were infected with ~100–200 CFU of Mtb by aerosol, using a whole-body Inhalation Exposure System (Glas-Col, Terre Haute, IN, USA). Briefly, a 5 ml single-cell suspension was aerosolized into a 5 ft^3 chamber over a period of 45 min, with compressed air and vacuum flow maintained at 10 and 60 ft^3/h, respectively. Three mice were sacrificed 24 h after aerosol exposure, and lungs processed as detailed in 'Quantitation of Mtb in tissues' below to confirm the pulmonary infection dose.

Quantitation of Mtb in tissues

Mice were euthanized by CO_2 asphyxiation at various times after infection. Lungs and spleens were aseptically removed and homogenized with steel beads in PBS + 0.05% Tween-80 using a Bullet Blender (Next Advance, Inc, Averill Park, NY, USA). Homogenates were serially diluted in PBS + 0.05% Tween-80 and spread on Middlebook 7H11 agar (BD Biosciences) supplemented with 0.5% (v/v) glycerol and 10% (v/v) OADC supplements (50 g/l bovine serum albumin, 20 g/l dextrose, 0.04 g/l catalase and 0.5 g/l oleic acid [Sigma-Aldrich]). Colonies were counted following incubation for 21 days at 37 °C, and were expressed as CFU/organ.

Bronchoalveolar lavage

Bronchoalveolar lavage was performed to obtain alveolar macrophages. Briefly, mice were euthanized as above, and the trachea exposed and cannulated with an 18-gauge needle. Lungs were lavaged with eight 1 ml aliquots of sterile ice-cold Hank's Balanced Salt Solution (Ca-/Mg-free) containing 0.5 mM EDTA. Retrieved cells were cultured in tissue culture-treated plates for 45 min to allow alveolar macrophages to adhere. Non-attached cells were discarded, and plates washed three times with PBS. Macrophages were detached with trypsin-EDTA (Sigma-Aldrich), washed with PBS and lysed with cell lysis buffer.

Measurement of lung cytokines

A portion of the lung homogenate from each animal (prepared for CFU determination) was diluted 1:1 with cell lysis buffer and immediately frozen at −80 °C until analysis. Diluted homogenates were thawed and centrifuged at $9000 \times g$ for 10 min to remove debris. TNF and IL-1β levels in the supernatants of centrifuged homogenates were determined by ELISA (Elisakit.com, Scoresby, Australia), according to the manufacturer's instructions. Data were expressed as pg of cytokine/ml of homogenate.

Lung histology and immunostaining

Lungs were inflated by intratracheal perfusion of 4% paraformaldehyde, and lungs and spleens fixed overnight at 4 °C. Left lobes and spleens were embedded in paraffin, sectioned, and stained with either haematoxylin and eosin (H&E), or immunohistochemically with rat anti-mouse F4/80 (WEHI) or rabbit anti-human MLKL (phospho S358) (EPR9514; Abcam) using the automated Omnis EnVision G2 template (Dako, Glostrup, Denmark). Dewaxing was performed with Clearify Clearing Agent (Dako) for 15 min, and antigen retrieval with EnVision FLEX TRS, High pH (Dako) at 97 °C for 30 min. Primary antibodies were diluted in EnVision Flex Antibody Diluent (Dako) and incubated at 32 °C for 60 min. HRP-labelled secondary antibodies were applied at 32 °C for 20 min. Slides were counter-stained with Mayer Hematoxylin, dehydrated, cleared, and mounted with MM24 Mounting Medium (Surgipath-Leica, Buffalo Grove, IL, USA). Slides were scanned with an Aperio ScanScope AT slide scanner (Leica Microsystems, Wetzlar, Germany) or imaged with an Eclipse 90i microscope (Nikon, Tokyo, Japan).

Following fixation, right lung lobes were dehydrated in 30% sucrose in PBS at 4 °C for several days, embedded in Tissue-Tek Optimal Cutting Temperature (Sakura Finetek, Torrance, CA, USA) media, and rapidly frozen. Immunostaining was performed on 6 µm cryosections on poly-L-lysine glass slides. Thawed slides were rehydrated using TBS and blocked with a solution of 10% goat serum (Abcam) in TBS for 1 h at room temperature. Primary antibodies were applied sequentially with overnight incubations at 4 °C. Slides were initially stained with antibodies targeting CD3 (rabbit anti-CD3; 1:200; Dako), followed by staining for 1 h with a secondary antibody (goat anti-rabbit AF594-conjugated; 1:200; Molecular Probes, Eugene, OR, USA). Slides were subsequently stained with primary antibodies targeting CD4 (rat anti-CD4 AF647-conjugated; 1:50; Life Technologies), followed by staining with DAPI (300 nM, Molecular Probes) for 5 min. Slides were washed three times with TBS between each staining. Coverslips were mounted using ProLong Gold antifade (Molecular Probes). Slides were visualized on a Zeiss AxioObserver.Z1 Confocal Microscope (Carl Zeiss Microsystems, Jena, Germany) with a 20x N.A. dry objective. A 4×4 tile scan with z stacking was performed around inflammatory lesions. A maximum intensity projection was applied to tile scans, which were then stitched using Zen software (Carl Zeiss Microsystems).

Immune cell extraction and flow cytometry

Lungs were transcardially perfused with ice-cold RPMI, minced with scalpel blades and digested with 3 mg/ml collagenase III (Worthington, Freehold, NJ, USA) and 2 mg/ml DNase I (Roche) for 90 min at 37 °C with frequent vortexing. Digested lung tissue was mashed through a 70 µm strainer, washed with PBS + 2% FCS and resuspended in 40% Percoll (GE Healthcare) before centrifugation at 900 *g* for 10 min. Debris and Percoll were removed and cell pellets treated with ACK red cell lysis buffer (150 mM NH_4Cl, 10 mM $KHCO_3$ and 0.1 mM EDTA). Spleens were mashed through a 40 µm strainer and treated with ACK. A portion of isolated lung cells and splenocytes were Fc blocked with anti-CD16/CD32 (BD Biosciences) for 20 min at room temperature and then stained with the following antibodies (all from BD Biosciences) for 30 min at 4 °C: rat anti-CD4 BV421 (GK1.5), rat anti-CD8 PE-Cy7 (53–6.7), rat anti-CD19 PerCP-Cy5.5 (1D3), rat anti-CD11b BV510 (M1/70), hamster anti-CD11c APC (HL3), rat anti-I-A/I-E (2G9) FITC, and rat anti-Ly-6G/Ly-6C PE (RB6–8C5). Stained cells were analyzed using a FACSAria Fusion flow cytometer (BD Biosciences).

Ex vivo peptide restimulation

Approximately 2×10^6 splenocytes and 3×10^6 lung cells were cultured in 24-well plates in Iscove's modified Dulbecco's medium (IMDM) containing 10% FCS, β-mercaptoethanol, penicillin/streptomycin, GolgiStop and GolgiPlug (BD Biosciences). Cells were stimulated with either 50 ng/ml phorbol 12-myristate 13-acetate (PMA, Sigma-Aldrich) and 650 nM ionomycin (Sigma-Aldrich) as a positive control, 100 nM chicken ovalbumin (OVA; ISQAVHAAHAEINEAGR) peptide (GenScript, Piscataway, NJ, USA) or 5 µg/ml Mtb early secreted antigenic target 6 (ESAT-6; MTEQQWNFAGIEAAA) peptide (GenScript), and incubated for 5 h. Cells were then harvested, Fc blocked, surface stained with rat anti-CD4 BV421 and rat anti-CD8 PE-Cy7, fixed and permeabilized (Fixation/Permeabilization reagent and Permeabilization Buffer; eBioscience, San Diego, CA, USA). Intracellular cytokine staining was performed by incubating cells with rat anti-TNF PE (MP6-XT22; Biolegend) and rat anti-IFNγ FITC (XMG1.2; BD Biosciences) for 45 min at 4 °C. Stained cells were analyzed using a FACSAria Fusion flow cytometer (BD Biosciences).

LCMV infection

Humanized mice were infected intravenously with 2×10^6 PFU LCMV docile strain. Seven days after infection, mice were treated by IP injection with 60 mg/kg emricasan, either alone or in combination with 10 mg/kg Nec-1s. This was followed 20 min later by IP injection of 30 mg/kg birinapant. A subsequent dose of emricasan was given 2 h following the initial dose. Mice were sacrificed 3 h after administration of birinapant.

Statistical and image analyses

Prism 6.0 h (GraphPad Software, San Diego, CA, USA) was used to perform statistical tests. Groups were compared by either unpaired two-tailed *t* tests for parametric data, or Mann–Whitney tests for non-parametric data. Microscopy images were processed using FIJI software and analyzed quantitatively with custom-written macros.

Acknowledgements We thank James Vince, James Murphy and Najoua Lalaoui for discussions, Lachlan Whitehead and the Centre for Dynamic Imaging for assistance with image analysis, Benjamin Kile for supplying *Ifnar1*$^{-/-}$ mice, the Australian Red Cross Blood Service for supplying buffy packs and Liana Mackiewicz for technical support. This work was supported by National Health and Medical Research Council Australia (Grants 1006592, 1045549 and 1065626 to MP, 1039014 to SP, 1056282 to SO, 1016647 and 1058344 to WSA, and 1057905 and 1058190 to JS), The Sylvia & Charles Viertel Senior Medical Research Fellowship (M. P.), the Victorian State Government Operational Infrastructure Support and the Independent Research Institutes Infrastructure Support Scheme of the Australian Government National Health and Medical Research Council. The Walter and Eliza Hall Institute of Medical Research have a research license agreement with TetraLogic Pharmaceuticals (Malvern, PA, USA), the manufactures of the cIAP antagonist birinapant. MP and JS provided consultative advice to, and were on the scientific advisory board of, TetraLogic Pharmaceuticals.

Compliance with ethical standards

Conflict of interest The authors declare that they have no competing interests.

Open Access This article is licensed under a Creative Commons Attribution-NonCommercial-ShareAlike 4.0 International License, which permits any non-commercial use, sharing, adaptation, distribution and reproduction in any medium or format, as long as you give appropriate credit to the original author(s) and the source, provide a link to the Creative Commons license, and indicate if changes were made. If you remix, transform, or build upon this article or a part thereof, you must distribute your contributions under the same license as the original. The images or other third party material in this article are included in the article's Creative Commons license, unless indicated otherwise in a credit line to the material. If material is not included in the article's Creative Commons license and your intended use is not permitted by statutory regulation or exceeds the permitted use, you will need to obtain permission directly from the copyright holder. To view a copy of this license, visit http://creativecommons.org/licenses/by-nc-sa/4.0/.

References

1 Meena LS, Rajni. Survival mechanisms of pathogenic mycobacterium tuberculosis H37Rv. FEBS J 2010;277:2416–27.
2 Aporta A, Arbues A, Aguilo JI, Monzon M, Badiola JJ, de Martino A, et al. Attenuated Mycobacterium tuberculosis SO2 vaccine candidate is unable to induce cell death. PLoS ONE 2012;7:e45213.

3 Aguilo JI, Alonso H, Uranga S, Marinova D, Arbués A, Martino A, et al. ESX-1-induced apoptosis is involved in cell-to-cell spread of Mycobacterium tuberculosis. Cell Microbiol 2013;15:1994–2005.
4 Aguiló N, Uranga S, Marinova D, Martín C, Pardo J. Bim is a crucial regulator of apoptosis induced by Mycobacterium tuberculosis. Cell Death Dis 2014;5:e1343.
5 Derrick SC, Morris SL. The ESAT6 protein of Mycobacterium tuberculosis induces apoptosis of macrophages by activating caspase expression. Cell Microbiol 2007;9:1547–55.
6 Davis JM, Ramakrishnan L. The role of the granuloma in expansion and dissemination of early tuberculous infection. Cell 2009;136:37–49.
7 Keane J, Remold HG, Kornfeld H. Virulent Mycobacterium tuberculosis strains evade apoptosis of infected alveolar macrophages. J Immunol 2000;164:2016–20.
8 Balcewicz-Sablinska MK, Keane J, Kornfeld H, Remold HG. Pathogenic Mycobacterium tuberculosis evades apoptosis of host macrophages by release of TNF-R2, resulting in inactivation of TNF-alpha. J Immunol. 1998;161:2636–41.
9 Riendeau CJ, Kornfeld H. THP-1 cell apoptosis in response to Mycobacterial infection. Infect Immun 2003;71:254–9.
10 Dhiman R, Raje M, Majumdar S. Differential expression of NF-kappaB in mycobacteria infected THP-1 affects apoptosis. Biochim Biophys Acta 2007;1770:649–58.
11 Keane J, Balcewicz-Sablinska MK, Remold HG, Chupp GL, Meek BB, Fenton MJ, et al. Infection by Mycobacterium tuberculosis promotes human alveolar macrophage apoptosis. Infect Immun. 1997;65:298–304.
12 Sly LM, Hingley-Wilson SM, Reiner NE, McMaster WR. Survival of Mycobacterium tuberculosis in host macrophages involves resistance to apoptosis dependent upon induction of antiapoptotic Bcl-2 family member Mcl-1. J Immunol 2003;170:430–7.
13 Velmurugan K, Chen B, Miller JL, Azogue S, Gurses S, Hsu T, et al. Mycobacterium tuberculosis nuoG is a virulence gene that inhibits apoptosis of infected host cells. PLoS Pathog 2007; 3:e110.
14 Hinchey J, Lee S, Jeon BY, Basaraba RJ, Venkataswamy MM, Chen B, et al. Enhanced priming of adaptive immunity by a proapoptotic mutant of Mycobacterium tuberculosis. J Clin Invest 2007;117:2279–88.
15 Poirier V, Bach H, Av-Gay Y. Mycobacterium tuberculosis promotes anti-apoptotic activity of the macrophage by PtpA protein-dependent dephosphorylation of host GSK3α. J Biol Chem 2014; 289: 29376–85.
16 Behar SM, Martin CJ, Booty MG, Nishimura T, Zhao X, Gan H-X, et al. Apoptosis is an innate defense function of macrophages against Mycobacterium tuberculosis. Mucosal Immunol 2011;4:279–87.
17 Oddo M, Renno T, Attinger A, Bakker T, MacDonald HR, Meylan PR. Fas ligand-induced apoptosis of infected human macrophages reduces the viability of intracellular Mycobacterium tuberculosis. J Immunol. 1998;160:5448–54.
18 Gan H, Lee J, Ren F, Chen M, Kornfeld H, Remold HG. Mycobacterium tuberculosis blocks crosslinking of annexin-1 and apoptotic envelope formation on infected macrophages to maintain virulence. Nat Immunol 2008;9:1189–97.
19 Lee J, Remold HG, Ieong MH, Kornfeld H. Macrophage apoptosis in response to high intracellular burden of Mycobacterium tuberculosis is mediated by a novel caspase-independent pathway. J Immunol 2006;176:4267–74.
20 Park JS, Tamayo MH, Gonzalez-Juarrero M, Orme IM, Ordway DJ. Virulent clinical isolates of Mycobacterium tuberculosis grow rapidly and induce cellular necrosis but minimal apoptosis in murine macrophages. J Leukoc Biol 2006;79:80–6.
21 Roca FJ, Ramakrishnan L. TNF dually mediates resistance and susceptibility to mycobacteria via mitochondrial reactive oxygen species. Cell 2013;153:521–34.
22 Zhao J, Jitkaew S, Cai Z, Choksi S, Li Q, Luo J, et al. Mixed lineage kinase domain-like is a key receptor interacting protein 3 downstream component of TNF-induced necrosis. Proc Natl Acad Sci USA 2012;109:5322–7.
23 Sun L, Wang H, Wang Z, He S, Chen S, Liao D, et al. Mixed lineage kinase domain-like protein mediates necrosis signaling downstream of RIP3 kinase. Cell 2012;148:213–27.
24 Zhao X, Khan N, Gan H, Tzelepis F, Nishimura T, Park S-Y, et al. Bcl-xL mediates RIPK3-dependent necrosis in M. tuberculosis-infected macrophages. Mucosal Immunol 2017;8:668.
25 Tobin DM, Roca FJ, Oh SF, McFarland R, Vickery TW, Ray JP, et al. Host genotype-specific therapies can optimize the inflammatory response to mycobacterial infections. Cell 2012;148:434–46.
26 Keane J, Gershon S, Wise RP, Mirabile-Levens E, Kasznica J, Schwieterman WD, et al. Tuberculosis associated with infliximab, a tumor necrosis factor alpha-neutralizing agent. N Engl J Med 2001;345:1098–1104.
27 Flynn JL, Goldstein MM, Chan J, Triebold KJ, Pfeffer K, Lowenstein CJ, et al. Tumor necrosis factor-alpha is required in the protective immune response against Mycobacterium tuberculosis in mice. Immunity. 1995;2:561–72.
28 Murphy JM, Czabotar PE, Hildebrand JM, Lucet IS, Zhang J-G, Alvarez-Diaz S, et al. The pseudokinase MLKL mediates necroptosis via a molecular switch mechanism. Immunity 2013;39:443–53.
29 Hildebrand JM, Tanzer MC, Lucet IS, Young SN, Spall SK, Sharma P, et al. Activation of the pseudokinase MLKL unleashes the four-helix bundle domain to induce membrane localization and necroptotic cell death. Proc Natl Acad Sci USA 2014;111:15072–7.
30 Chen X, Li W, Ren J, Huang D, He W-T, Song Y, et al. Translocation of mixed lineage kinase domain-like protein to plasma membrane leads to necrotic cell death. Cell Res 2014;24:105–21.
31 Huang D, Zheng X, Wang Z-A, Chen X, He W-T, Zhang Y et al. MLKL channel in necroptosis is octamer formed by tetramers in a dyadic process. Mol Cell Biol 2016: MCB. 00497–16. 37: e00497-16
32 Wang H, Sun L, Su L, Rizo J, Liu L, Wang L-F, et al. Mixed lineage kinase domain-like protein MLKL causes necrotic membrane disruption upon phosphorylation by RIP3. Mol Cell 2014;54:133–46.
33 Upton JW, Kaiser WJ, Mocarski ES. DAI/ZBP1/DLM-1 complexes with RIP3 to mediate virus-induced programmed necrosis that is targeted by murine cytomegalovirus vIRA. Cell Host Microbe 2012;11:290–7.
34 He S, Liang Y, Shao F, Wang X. Toll-like receptors activate programmed necrosis in macrophages through a receptor-interacting kinase-3-mediated pathway. Proc Natl Acad Sci USA 2011;108:20054–9.
35 Omoto S, Guo H, Talekar GR, Roback L, Kaiser WJ, Mocarski ES. Suppression of RIP3-dependent necroptosis by human cytomegalovirus. J Biol Chem 2015;290:11635–48.
36 Guo H, Omoto S, Harris PA, Finger JN, Bertin J, Gough PJ, et al. Herpes simplex virus suppresses necroptosis in human cells. Cell Host Microbe 2015;17:243–51.
37 Ma W, Tummers B, van Esch EMG, Goedemans R, Melief CJM, Meyers C, et al. Human papillomavirus downregulates the expression of IFITM1 and RIPK3 to escape from IFNγ- and TNFα-mediated antiproliferative effects and necroptosis. Front Immun 2016;7:496.
38 Li S, Zhang L, Yao Q, Li L, Dong N, Rong J, et al. Pathogen blocks host death receptor signalling by arginine GlcNAcylation of death domains. Nature 2013;501:242–6.

39 Danelishvili L, Yamazaki Y, Selker J, Bermudez LE. Secreted Mycobacterium tuberculosis Rv3654c and Rv3655c proteins participate in the suppression of macrophage apoptosis. PLoS ONE 2010;5:e10474.

40 Legarda D, Justus SJ, Ang RL, Rikhi N, Li W, Moran TM, et al. CYLD proteolysis protects macrophages from TNF-mediated autonecroptosis induced by LPS and licensed by type I IFN. Cell Rep 2016;15:2449–61.

41 Murphy JM, Silke J. Ars Moriendi; the art of dying well - new insights into the molecular pathways of necroptotic cell death. EMBO Rep 2014;15:155–64.

42 Moquin DM, McQuade T, Chan FK-M. CYLD deubiquitinates RIP1 in the TNFα-induced necrosome to facilitate kinase activation and programmed necrosis. PLoS ONE 2013;8:e76841.

43 Degterev A, Hitomi J, Germscheid M, Ch'en IL, Korkina O, Teng X, et al. Identification of RIP1 kinase as a specific cellular target of necrostatins. Nat Chem Biol 2008;4:313–21.

44 Takahashi N, Duprez L, Grootjans S, Cauwels A, Nerinckx W, DuHadaway JB, et al. Necrostatin-1 analogues: critical issues on the specificity, activity and in vivo use in experimental disease models. Cell Death Dis 2012;3:e437.

45 MacMicking JD, North RJ, LaCourse R, Mudgett JS, Shah SK, Nathan CF. Identification of nitric oxide synthase as a protective locus against tuberculosis. Proc Natl Acad Sci USA. 1997;94:5243–8.

46 Periasamy S, Le HT, Duffy EB, Chin H, Harton JA. Inflammasome-independent NLRP3 restriction of a protective early neutrophil response to pulmonary tularemia. PLoS Pathog 2016;12:e1006059.

47 Kitur K, Wachtel S, Brown A, Wickersham M, Paulino F, Peñaloza HF, et al. Necroptosis promotes Staphylococcus aureus clearance by inhibiting excessive inflammatory signaling. Cell Rep 2016;16:2219–30.

48 Wang Q, Zhou T, Liu Z, Ren J, Phan N, Gupta K, et al. Inhibition of Receptor-Interacting Protein Kinase 1 with Necrostatin-1s ameliorates disease progression in elastase-induced mouse abdominal aortic aneurysm model. Sci Rep 2017;7:42159.

49 Huang Z, Epperly M, Watkins SC, Greenberger JS, Kagan VE, Bayır H. Necrostatin-1 rescues mice from lethal irradiation. Biochim Biophys Acta 2016;1862:850–6.

50 Ebert G, Preston S, Allison C, Cooney J, Toe JG, Stutz MD, et al. Cellular inhibitor of apoptosis proteins prevent clearance of hepatitis B virus. Proc Natl Acad Sci USA 2015;112:5797–802.

51 Heuts F, Gavier-Widén D, Carow B, Juarez J, Wigzell H, Rottenberg ME. CD4+ cell-dependent granuloma formation in humanized mice infected with mycobacteria. Proc Natl Acad Sci USA 2013;110:6482–7.

52 Hughes MA, Powley IR, Jukes-Jones R, Horn S, Feoktistova M, Fairall L, et al. Co-operative and hierarchical binding of c-FLIP and caspase-8: a unified model defines how c-FLIP isoforms differentially control cell fate. Mol Cell 2016;61:834–49.

53 Lin Y, Devin A, Rodriguez Y, Liu ZG. Cleavage of the death domain kinase RIP by caspase-8 prompts TNF-induced apoptosis. Genes Dev. 1999;13:2514–26.

54 Feng S, Yang Y, Mei Y, Ma L, Zhu D-E, Hoti N, et al. Cleavage of RIP3 inactivates its caspase-independent apoptosis pathway by removal of kinase domain. Cell Signal 2007;19:2056–67.

55 O'Donnell MA, Perez-Jimenez E, Oberst A, Ng A, Massoumi R, Xavier R, et al. Caspase 8 inhibits programmed necrosis by processing CYLD. Nat Cell Biol 2011;13:1437–42.

56 Oberst A, Dillon CP, Weinlich R, McCormick LL, Fitzgerald P, Pop C, et al. Catalytic activity of the caspase-8-FLIP(L) complex inhibits RIPK3-dependent necrosis. Nature 2011;471:363–7.

57 Tsuchiya Y, Nakabayashi O, Nakano H. FLIP the switch: regulation of apoptosis and necroptosis by cFLIP. IJMS 2015;16:30321–41.

58 Bonnet MC, Preukschat D, Welz P-S, van Loo G, Ermolaeva MA, Bloch W, et al. The adaptor protein FADD protects epidermal keratinocytes from necroptosis in vivo and prevents skin inflammation. Immunity 2011;35:572–82.

59 Witt A, Vucic D. Diverse ubiquitin linkages regulate RIP kinases-mediated inflammatory and cell death signaling. Cell Death Differ 2017;24:1160–71.

60 Hwang SY, Hertzog PJ, Holland KA, Sumarsono SH, Tymms MJ, Hamilton JA, et al. A null mutation in the gene encoding a type I interferon receptor component eliminates antiproliferative and antiviral responses to interferons alpha and beta and alters macrophage responses. Proc Natl Acad Sci USA. 1995;92:11284–8.